PROCEEDINGS OF SCIENCE

ONLINE ICRC 2021
THE ASTROPARTICLE PHYSICS CONFERENCE
Berlin | Germany
37th International Cosmic Ray Conference
12–23 July 2021

Resolving the origin of very-high-energy gamma-ray emission from the PeVatron candidate SNR G106.3+2.7 using MAGIC telescopes

T. Oka,[a,*] **T. Saito,**[b] **H. Kubo**[a] **and M. Strzys**[b] **on behalf of the MAGIC Collaboration**[†]

[a] *Department of Physics and Astronomy, Kyoto University, Kyoto, 606-8502, Japan*
[b] *Institute for Cosmic Ray Research, The University of Tokyo, Chiba, 277-8582, Japan*

E-mail: oka.tomohiko.25n@st.kyoto-u.ac.jp

The supernova remnant (SNR) G106.3+2.7 associated with a 100 TeV gamma-ray source reported by HAWC, Tibet ASγ, and LHAASO Collaborations is one of the promising PeVatron candidates. Because the SNR contains an energetic pulsar wind nebula (PWN) dubbed Boomerang powered by the pulsar PSR J2229+6114, it is unclear whether the gamma-ray emission originates from the SNR or PWN complex and whether it is caused by hadronic or leptonic processes. We observed gamma rays above 200 GeV in the vicinity of the SNR G106.3+2.7 using the MAGIC telescopes for total $\sim$ 120 hours between May 2017 and August 2019 with an angular resolution of 0.07–0.10 degrees, achieving an unprecedented exposure for this object at these energies. An extended gamma-ray emission spatially correlated with the radio continuum emission at the head and tail of SNR G106.3+2.7 was detected using the MAGIC telescopes. We found a significant gamma-ray emission above 5.65 TeV only from the SNR tail region, while no significant emission in the same band is found at the SNR head region containing the Boomerang PWN. Therefore, the gamma rays above 10 TeV detected with the air shower experiments are, likely, mainly emitted from the SNR tail region. In this presentation, we discuss the morphology of the gamma-ray emission from this complex region and attempt self-consistent multi-wavelength modeling of the energy spectrum.

37th International Cosmic Ray Conference (ICRC 2021)
July 12th – 23rd, 2021
Online – Berlin, Germany

*Presenter
†a complete list of the MAGIC Collaboration authors can be found at the end of the proceedings

PoS(ICRC2021)796

1. Introduction

Supernova remnants (SNRs) in our Galaxy are believed to be cosmic-ray accelerators up to PeV energies, and are commonly referred to as "PeVatrons" [1]. An observation of gamma rays above 100 TeV is a reliable (actually only reliable when emission is proven to be hadronic) method to confirm the potential PeVatron. Recent observations by air shower experiments have revealed 100 TeV gamma-ray emissions from SNR G106.3+2.7. Observations in the vicinity of SNR G106.3+2.7 by HAWC and Tibet ASγ experiments observed a gamma-ray spectrum without an exponential cutoff up to 100 TeV, providing a lower limit on the maximum energy of the accelerated particles, 270^{+140}_{-170} TeV [2] or 190 TeV [3] for electrons and 800^{+990}_{-640} TeV [2] or 500 TeV [3] for protons. In addition, LHAASO experiment detected a gamma-ray spectrum with more statistics, providing the photon cutoff energy of 570 ± 190 TeV [4]. However, an interpretation of the very-high-energy (VHE) gamma-ray emissions from this region is still challenging because SNR G106.3+2.7 contains an energetic pulsar accompanied with GeV pulse emissions [5] and a pulsar wind nebula (PWN) G106.6+2.9 named Boomerang [6].

SNR G106.3+2.7 has a comet-like shape and consists two patches called head (G106.58+2.86) and tail (G106.10+2.73) in the radio continuum band [7]. X-ray observations revealed non-thermal X-ray emissions from this SNR [8, 9], and one of the observations suggests that SNR-head originates from electrons escaped from the PWN [8]. In the gamma-ray band, the angular resolution of previous gamma-ray observations has not been sufficient to resolve the PWN or SNR components. Hence, it is unclear whether the gamma-ray emission originates from the SNR or PWN complex and whether it is caused by hadronic or leptonic processes. With an aim to resolve the origin of the VHE gamma-ray emission, we study this complex region using 122 hours of MAGIC data.

2. MAGIC observations

The MAGIC (Major Atmospheric Gamma Imaging Cherenkov) telescope is a system of two 17 m diameter imaging Cherenkov telescopes located in the Canary island La Palma, Spain (28.76° N; 17.89° W). MAGIC is capable of observing gamma-ray induced extensive air showers in the atmosphere via their Cherenkov light. At medium Zenith angles (30–45 deg), it can detect sources as weak as $(0.76 \pm 0.04)\%$ of the Crab Nebula flux at 5σ significance level above 0.21 TeV within 50 hours [10]. The gamma-ray observations in the vicinity of SNR G106.3+2.7 were performed between May 2017 and August 2019 at zenith angles between 30 and 50 degrees, yielding an analysis energy threshold of ∼0.2 TeV. The MAGIC angular resolution, characterised by the point spread function (PSF), for this analysis is estimated to be 0.084 degree (68% containment radius) at $E > 0.2$ TeV and 0.072 degree at $E > 1$ TeV, which is the best angular resolution among the previous gamma-ray observations for this object. To measure the background data simultaneously, we observed this region in wobble mode [11] at three positions (α = 336.°31, δ = 61.°40; α = 338.°25, δ = 61.°06; α = 336.°66, δ = 60.°42) with an offset of 0.57 degree from a position close to the center of VERITAS source (α = 337.°05, δ = 60.°96). In this analysis the standard MAGIC analysis and reconstruction software [12] is used. To suppress the systematic effects caused by the atmospheric condition, we selected data with the atmospheric transmission above 85% based on the LIDAR system [13]. After applying these quality cuts, the total live-time is ∼122 hours.

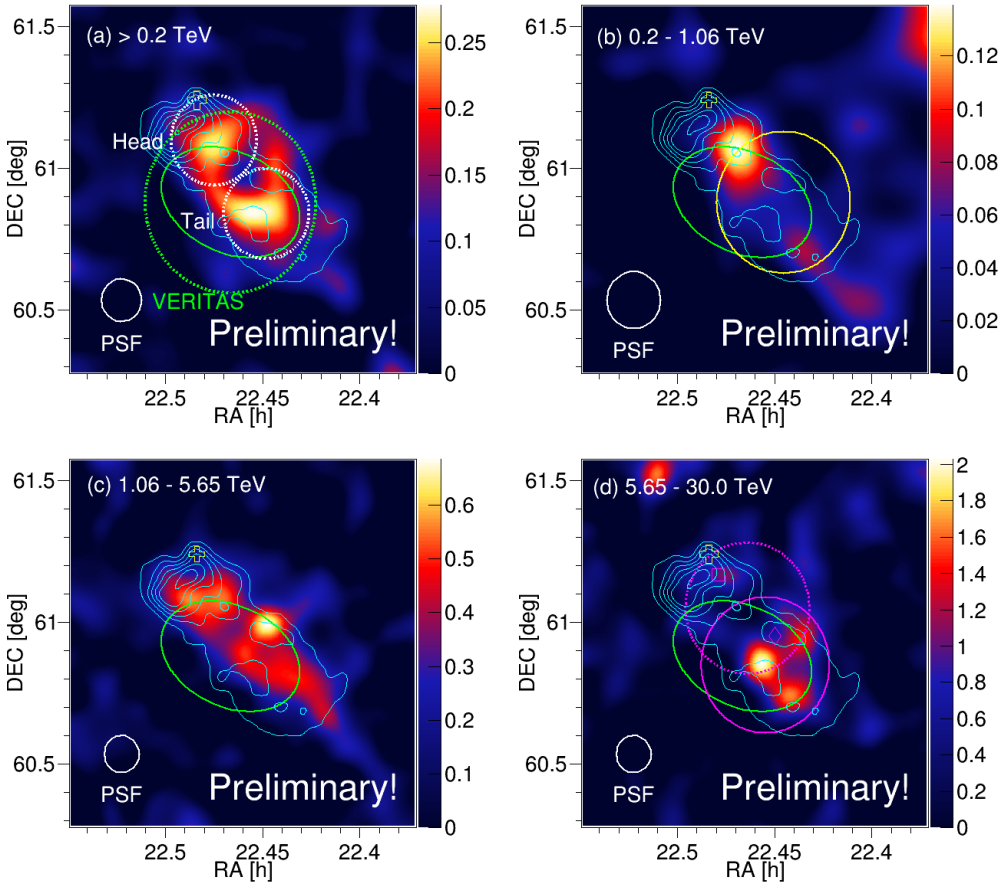

Figure 1: MAGIC relative flux (excess events over background events) maps in the vicinity of SNR G106.3+2.7. The energy ranges are for (a) >0.2 TeV (b) 0.2–1.06 TeV, (c) 1.06–5.65 TeV and (d) 5.65–30.0 TeV, respectively. All maps are smoothed with a Gaussian kernel, the size of which are shown with the white circle labeled PSF. In all panels, the open yellow cross represents the position of PSR J2229.0+6114. The cyan contours show the radio emission of SNR G106.3+2.7 at 408 MHz by DRAO [6]. The green ellipse represents the extended TeV gamma-ray emission of VER J2227+608 [14]. In panel (a), the white and green dotted circles represent θ^2 cut regions for the head, tail regions, and that used in the VERITAS paper [14], respectively. In panel (b), the yellow circle represents an extension of the Fermi-LAT source [15]. In panel (d), the magenta dotted and solid circle represent the upper limit at 90% confidence level of the Gaussian extension of HAWC J2227+610 [2] and the extended gamma-ray emission above 10 TeV observed with Tibet ASγ [3]. The open square and diamond show the centroid of the VHE emission detected with Milagro [16] and LHAASO [4], respectively.

3. Results

Figure 1(a) shows a relative flux map in the vicinity of SNR G106.3+2.7 above 0.2 TeV. The gamma-ray emissions extend and spatially coincide with the radio continuum emission from the SNR as shown with the cyan contours. To clarify the extended gamma-ray emission, we analyzed two regions, Head and Tail, as defined in Table 1. The center positions of these regions are obtained by fitting a double symmetric Gaussian to the gamma-ray map above 0.2 TeV (Fig. 1 (a)). The radii

Table 1: Regions considered in this work for the analysis and the detection significance evaluated using a method of [17], in the two energy ranges of (i) >0.2 TeV and (ii) 5.65–30 TeV.

Source	RA	DEC	Radius	(i) >0.2 TeV	(ii) 5.65–30 TeV
Head region	337.°13	61.°10	0.°16	6.2σ	2.4σ
Tail region	336.°72	60.°84	0.°16	6.9σ	6.5σ

are chosen maximizing the extraction regions without overlapping with each other. The detection significances of each region were evaluated using a method of [17]. The gamma-ray excesses above 0.2 TeV are detected in both regions above 6σ confidence level (see Table 1). Figure 1(b-d) show the energy-dependent skymaps in the energy ranges for (b) 0.2–1.06 TeV, (c) 1.06–5.65 TeV and (d) 5.65–30.0 TeV, respectively. In panel (d) the significant emission is visible only in the tail region. In the higher band for 5.65–30 TeV, the gamma-ray emission in the tail region is detected with 6.5σ confidence level, in contrast, no significant emission is found in the head region (2.4σ).

We extracted the gamma-ray spectra of each region. Fig. 2 shows the gamma-ray spectra of the two regions defined in Table 1. The spectra were fitted by a single power-law function of $dN/dE = N_0(E/3\mathrm{TeV})^{-\Gamma}$. The best-fit parameters are $N_0 = (3.8 \pm 0.7_{\mathrm{stat}} \pm 0.7_{\mathrm{sys}}) \times 10^{-14}\mathrm{cm}^{-2}\mathrm{s}^{-1}\mathrm{TeV}^{-1}$ and $\Gamma = 2.12 \pm 0.12_{\mathrm{stat}} \pm 0.15_{\mathrm{sys}}$ for the head, while $N_0 = (6.0 \pm 0.7_{\mathrm{stat}} \pm 1.0_{\mathrm{sys}}) \times 10^{-14}\mathrm{cm}^{-2}\mathrm{s}^{-1}\mathrm{TeV}^{-1}$ and $\Gamma = 1.83 \pm 0.10_{\mathrm{stat}} \pm 0.15_{\mathrm{sys}}$ for the tail. Both differential flux and spectral index of the tail region are slightly larger and flatter than those of the head region, however in agreement within 2σ statistical uncertainty. The sum of differential flux of the head and tail is $N_0 = (9.8 \pm 0.9_{\mathrm{stat}} \pm 1.2_{\mathrm{sys}}) \times 10^{-14}\mathrm{cm}^{-2}\mathrm{s}^{-1}\mathrm{TeV}^{-1}$, which is consistent within 1σ statistical uncertainty with the VERITAS result ($(11.5 \pm 2.7_{\mathrm{stat}} \pm 3.5_{\mathrm{sys}}) \times 10^{-14}\mathrm{cm}^{-2}\mathrm{s}^{-1}\mathrm{TeV}^{-1}$) [14].

4. Discussion

In the previous observations, the location of the gamma-ray emissions suggested to be consistent with the SNR-tail region [e.g., 14, 15]. This analysis discovered significant gamma-ray emissions on both head and tail regions, which spatially coincide with the radio continuum emissions. Since the gamma-ray spectra in the head and tail regions are similar, the origins of these emissions might be considered from the same source. Several models have been already attempted to explain the gamma-ray emissions from the entire region of this SNR [e.g., 8, 9]. Some models show that the hadronic origin model is preferred to leptonic for the gamma-ray emission above 10 TeV [8, 19], however, leptonic emission remains as a possible explanation [9].

The center position of the tail region is in a good agreement with the peak positions of gamma-ray emissions reported > 10 TeV [2–4, 14]. There is the significant gamma-ray emission above 5.65 TeV from the tail in contrast with no significant emission from the head as shown in Fig. 1(d). This suggests that the gamma rays above 10 TeV detected with the air shower arrays [2, 3, 16] are mainly emitted from the tail region. Here, we tried to model the multi-wavelength spectrum of each region and interpret the origin of the VHE gamma-ray emissions under the assumption that the gamma-ray emissions above 10 TeV measured with the air shower experiments are only from the tail region.

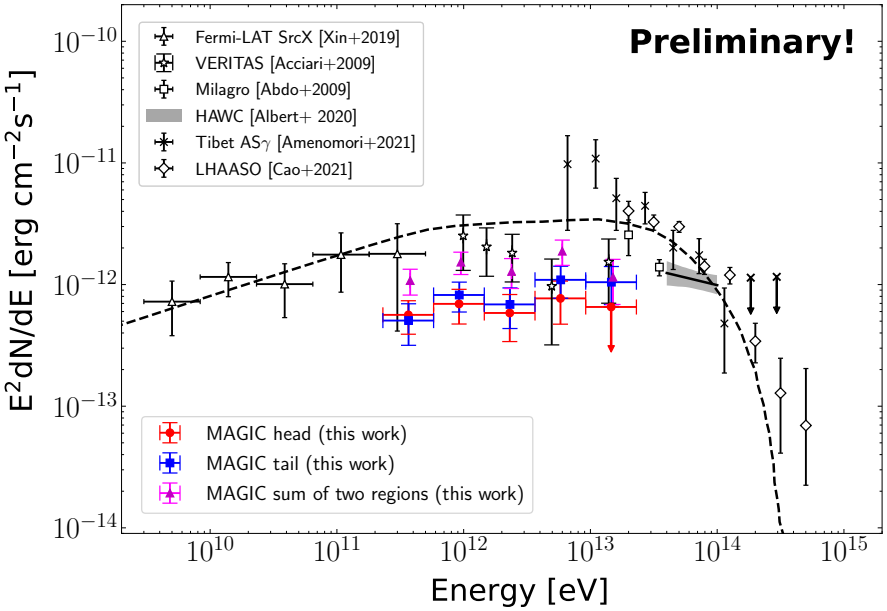

Figure 2: Gamma-ray spectra of the head (red), tail (blue) regions as measured with the MAGIC telescopes. The magenta triangles represent the total fluxes of head and tail. The open triangles, open stars, open squares, x marks, and open diamonds show the results for whole region of SNR G106.3+2.7 as measured with *Fermi*-LAT [15], VERITAS [14], Milagro [16, 18], Tibet ASγ [3], and LHAASO [4], respectively. The bow-tie area shows a power-law fit and 1σ statistical uncertainty measured with HAWC [2]. The black dotted line shows the lepto-hadronic model for the whole region (Model 1 in [19]).

4.1 Head region

The head region defined in this work contains the Boomerang PWN and the SNR-head. In particular, the X-ray observation of the SNR-head found a gradual softening of the spectrum with the distance from the pulsar, supporting leptonic origin escaped from the PWN. Therefore, we modeled the energy spectrum of the head region with the leptonic model. For the gamma-ray emission mechanism, the inverse Compton (IC) scatterings with cosmic microwave background and infrared emissions are only considered as the target photon field [20]. The energy densities of infrared emissions are estimated to 0.1 eV cm^{-3} at 30 K and 0.3 eV cm^{-3} at 3000 K using the package of GALPROP [21]. The Synchrotron radiation is also considered for the lower band. The modeling is performed by the naima package [22]. In this modeling, a distance to the SNR G106.3+2.7 from the Earth is assumed to be 0.8 kpc [23]. The data points in the radio band are adopted the SNR-head flux [6]. The X-ray spectra for the head region is taken from results of the "East" region [9], multiplying the intensity by the area of a circle with a radius of 0.16 degrees. Regarding the *Fermi*-LAT data, the spectrum of this SNR in an energy range of 3–500 GeV computed under the assumption of the spatial model of an uniform disk with radius of 0.25 degrees depicted in Fig. 1(b), which overlaps with the part of the head region as well as the tail region [15, 24]. Hence, we treated the flux as an upper limit on that of both region. The left panel of Figure 3 shows the modeling results for the head region. The magnetic field and total electron energy above 1 GeV are given to be 6 μG and 5.7×10^{46} erg, respectively. Electrons with an index of 2.5 and the cutoff

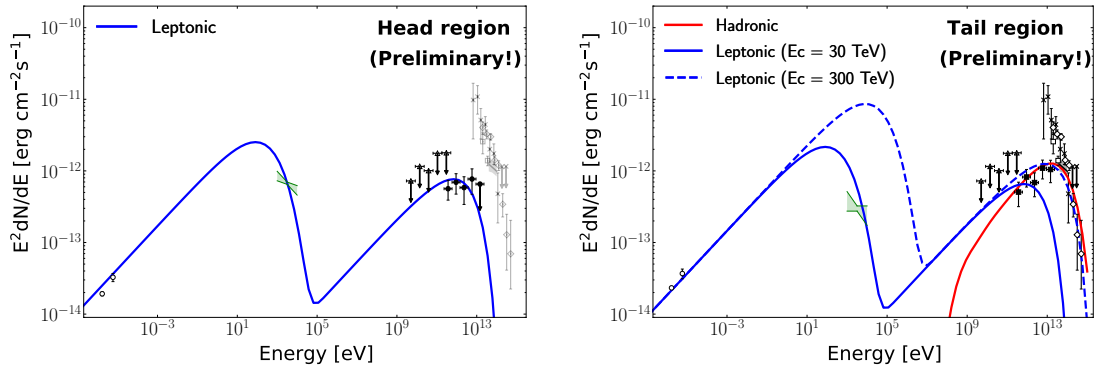

Figure 3: Modeling for the head and tail regions. The open circles show the data in the radio band [6]. The green bow-tie area shows a single power-law fit and 1σ statistical uncertainty measured by Suzaku [9] (see text). The markers in the gamma band is the same as in Figure 2.

energy of 30 TeV can reproduce the observed spectrum of the head region (χ^2/d.o.f = 2.57/5 with respect to the MAGIC data).

4.2 Tail region

We modeled the gamma-ray spectrum in the tail region with a leptonic model, as with the head region. The data points are treated almost the same as in the case of the head region. We used the SNR-tail flux in the radio band [6] and the X-ray flux of "West" region observed Suzaku [9], multiplying the intensity by the area of a circle with a radius of 0.16 degrees in the latter case. We found that the MAGIC spectrum in the tail region can be reproduced by leptonic emission model (χ^2/d.o.f = 11.2/5 with respect to the MAGIC data). The magnetic field, total electron energy above 1 GeV, a spectral index, and a cutoff energy are given to be 6 μG, 4.9×10^{46} erg, 2.4, and 30 TeV, respectively. However, to reproduce the flux measured by the air shower experiments requires a higher cutoff energy of $\sim$ 300 TeV in tension with the X-ray flux.

On the other hand, the overlap with the molecular clouds and the tail region suggests that hadronic origin of the gamma-ray emission [14]. We also modeled the spectrum of the tail with the hadronic emission under the assumption that gamma-ray emissions are produced pion decay via p-p interactions. The hadronic model emission is computed using naima package [22]. The red model curve as shown in the right panel of Figure 3 is found to be consistent with the observed spectrum (χ^2/d.o.f = 2.2/5 with respect to the MAGIC data). For the model parameters, the proton index of 1.7, the cutoff energy of 1 PeV, and total proton energy above 1 GeV of 8.2×10^{45} erg ($N_{\rm gas}/200\,{\rm cm}^{-3}$), are given. Although an age of this SNR is estimated to be 3.9–10 kyr [25, 26], the model requires the maximum energy of $\sim$ 1 PeV, expected to be archived in younger SNRs than 1 kyr [27]. The discrepancy could be explained with the CR-escape model that protons accelerated up to $\sim$ PeV energies at a young SNR escaped from the shock wave and illuminated the nearby clouds, inducing the gamma-ray emission [e.g. 28]. The CR-escape scenario also allows the harder index than 2.0 expected in DSA [e.g., 29, 30]

The assumption that the gamma-ray emissions above 10 TeV are emitted only from the tail region favor a proton acceleration up to $\sim$ 1 PeV in the SNR. However, the measurements above

10 TeV performed with the air shower experiments may include the gamma-ray emissions from the head region as well as tail, due to the insufficient angular resolution to resolve the two regions. Further observations with better angular resolution are required to measure the cutoff energy of each region more precisely.

5. Conclusion

We observed gamma-rays with high angular resolution derived from 122 hours in the vicinity of the SNR G106.3+2.7 using MAGIC telescopes. MAGIC detected ($> 6\sigma$ confidence level) the extended gamma-ray emissions spatially coincided with the radio continuum emission. We found that the significant gamma-ray emission in the energy range for 5.65–30 TeV is only in the tail region. This result suggests that the gamma-ray emissions above 10 TeV observed with the air shower experiments are most likely emitted from the SNR tail. By the modeling, the MAGIC spectra of the head and tail region could be reproduced with the leptonic emissions. Once we assumed that the emission above 10 TeV detected by air shower experiments are mainly emitted from the tail region, the leptonic model requires a higher cutoff energy of electrons in tension with the X-ray flux. Therefore, the hadronic model is favored to explain the emission from the tail. Further observations of gamma rays higher than 10 TeV with an angular resolution enough for resolving the two regions and quantitatively evaluate the difference of the cutoff energies between head and tail, are required to reveal better the VHE gamma-ray origin.

Acknowledgments

We acknowledge the support from the agencies and organizations listed here: https://magic.mpp.mpg.de/acknowledgments_ICRC2021.

References

[1] Baade, W. & Zwicky, F. *Proceedings of the National Academy of Science* 20 (1934), no. 5 254–259.

[2] HAWC Collaboration, Albert, A. et al. *Astrophys. J. Lett.* 896 (2020) L29.

[3] Tibet ASγ Collaboration, Amenomori, M. et al. *Nature Astron.* 5 (2021), no. 5 460–464.

[4] Cao, Z., Aharonian, F. A., et al. *Nature* 594 (2021), no. 7861 33–36.

[5] Fermi-LAT, Fermi Pulsar Timing Consortium Collaboration, Abdo, A. et al. *Astrophys. J.* 706 (2009) 1331–1340.

[6] Pineault, S. & Joncas, G. *The Astronomical Journal* 120 (2000), no. 6 3218–3225.

[7] Joncas, G. & Higgs, L. A. *Astronomy and Astrophysics, Suppl. Ser.* 82 (1990) 113–144.

[8] Ge, C., Liu, R.-Y., et al. *The Innovation* 2 (2021) 100118.

[9] Fujita, Y., Bamba, A., et al. *The Astrophysical Journal* 912 (2021), no. 2 133.

[10] MAGIC Collaboration, Aleksić, J. et al. *Astropart. Phys.* 72 (2016) 76–94.

[11] Fomin, V., Stepanian, A., et al. *Astropart. Phys.* 2 (1994) 137–150.

[12] Zanin, R. in *33rd International Cosmic Ray Conference*, p. 0773, 2013.

[13] MAGIC Collaboration, Fruck, C., Gaug, M., et al. in *Proceedings, 33rd International Cosmic Ray Conference (ICRC2013): Rio de Janeiro, Brazil, July 2-9, 2013*, p. 1054, 2014.

[14] VERITAS Collaboration, Acciari, V. A. et al. *Astrophys. J.* 703 (2009) L6–L9.

[15] Xin, Y., Zeng, H., et al. *The Astrophysical Journal* 885 (2019), no. 2 162.

[16] Abdo, A. A. et al. *Astrophys. J.* 700 (2009) L127–L131. [Erratum: Astrophys. J.703,L185(2009)].

[17] Li, T.-P. & Ma, Y.-Q. *Astrophys. J.* 272 (1983) 317–324.

[18] Abdo, A. et al. *Astrophys. J.* 664 (2007) L91–L94.

[19] Bao, Y. & Chen, Y. *arXiv e-prints* (2021) arXiv:2103.01814.

[20] Blumenthal, G. R. & Gould, R. J. *Reviews of Modern Physics* 42 (1970), no. 2 237–271.

[21] Vladimirov, A. E., Digel, S. W., et al. *Comput. Phys. Commun.* 182 (2011) 1156–1161.

[22] Zabalza, V. *Proc. of International Cosmic Ray Conference 2015* (2015) 922.

[23] Kothes, R., Uyaniker, B., & Pineault, S. *The Astrophysical Journal* 560 (2001), no. 1 236–243.

[24] Liu, S., Zeng, H., et al. *Astrophys. J.* 897 (2020), no. 2 L34.

[25] Kothes, R., Reich, W., & Uyanıker, B. *Astrophys. J.* 638 (2006), no. 1 225–233.

[26] Halpern, J., Camilo, F., et al. *Astrophys. J.* 552 (2001) L125.

[27] Ptuskin, V. S. & Zirakashvili, V. N. *Astron. Astrophys.* 403 (2003) 1–10.

[28] Aharonian, F. A. & Atoyan, A. M. *A&A* 309 (1996) 917–928.

[29] Bell, A. R. *Mon. Not. Roy. Astron. Soc.* 182 (1978) 147–156.

[30] Blandford, R. & Ostriker, J. *Astrophys. J. Lett.* 221 (1978) L29–L32.

The MAGIC Collaboration

V. A. Acciari[1], S. Ansoldi[2,41], L. A. Antonelli[3], A. Arbet Engels[4], M. Artero[5], K. Asano[6], D. Baack[7], A. Babić[8], A. Baquero[9], U. Barres de Almeida[10], J. A. Barrio[9], I. Batković[11], J. Becerra González[1], W. Bednarek[12], L. Bellizzi[13], E. Bernardini[14], M. Bernardos[11], A. Berti[15], J. Besenrieder[15], W. Bhattacharyya[14], C. Bigongiari[3], A. Biland[4], O. Blanch[5], H. Bökenkamp[7], G. Bonnoli[16], Ž. Bošnjak[8], G. Busetto[11], R. Carosi[17], G. Ceribella[15], M. Cerruti[18], Y. Chai[15], A. Chilingarian[19], S. Cikota[8], S. M. Colak[5], E. Colombo[1], J. L. Contreras[9], J. Cortina[20], S. Covino[3], G. D'Amico[15,42], V. D'Elia[3], P. Da Vela[17,43], F. Dazzi[3], A. De Angelis[11], B. De Lotto[2], M. Delfino[5,44], J. Delgado[5,44], C. Delgado Mendez[20], D. Depaoli[21], F. Di Pierro[21], L. Di Venere[22], E. Do Souto Espiñeira[5], D. Dominis Prester[23], A. Donini[2], D. Dorner[24], M. Doro[11], D. Elsaesser[7], V. Fallah Ramazani[25,45], A. Fattorini[7], M. V. Fonseca[9], L. Font[26], C. Fruck[15], S. Fukami[6], Y. Fukazawa[27], R. J. García López[1], M. Garczarczyk[14], S. Gasparyan[28], M. Gaug[26], N. Giglietto[22], F. Giordano[22], P. Gliwny[12], N. Godinović[29], J. G. Green[3], D. Green[15], D. Hadasch[6], A. Hahn[15], L. Heckmann[15], J. Herrera[1], J. Hoang[9,46], D. Hrupec[30], M. Hütten[15], T. Inada[6], K. Ishio[12], Y. Iwamura[6], I. Jiménez Martínez[20], J. Jormanainen[25], L. Jouvin[5], M. Karjalainen[1], D. Kerszberg[5], Y. Kobayashi[6], H. Kubo[31], J. Kushida[32], A. Lamastra[3], D. Lelas[29], F. Leone[3], E. Lindfors[25], L. Linhoff[7], S. Lombardi[3], F. Longo[2,47], R. López-Coto[11], M. López-Moya[9], A. López-Oramas[1], S. Loporchio[22], B. Machado de Oliveira Fraga[10], C. Maggio[26], P. Majumdar[33], M. Makariev[34], M. Mallamaci[11], G. Maneva[34], M. Manganaro[23], K. Mannheim[24], L. Maraschi[3], M. Mariotti[11], M. Martínez[5], D. Mazin[6,15], S. Menchiari[13], S. Mender[7], S. Mićanović[23], D. Miceli[2,49], T. Miener[9], J. M. Miranda[13], R. Mirzoyan[15], E. Molina[18], A. Moralejo[5], D. Morcuende[9], V. Moreno[26], E. Moretti[5], T. Nakamori[35], L. Nava[3], V. Neustroev[36], C. Nigro[5], K. Nilsson[25], K. Nishijima[32], K. Noda[6], S. Nozaki[31], Y. Ohtani[6], T. Oka[31], J. Otero-Santos[1], S. Paiano[3], M. Palatiello[2], D. Paneque[15], R. Paoletti[13], J. M. Paredes[18], L. Pavletić[23], P. Peñil[9], M. Persic[2,50], M. Pihet[15], P. G. Prada Moroni[17], E. Prandini[11], C. Priyadarshi[5], I. Puljak[29], W. Rhode[7], M. Ribó[18], J. Rico[5], C. Righi[3], A. Rugliancich[17], N. Sahakyan[28], T. Saito[6], S. Sakurai[6], K. Satalecka[14], F. G. Saturni[3], B. Schleicher[24], K. Schmidt[7], T. Schweizer[15], J. Sitarek[12], I. Šnidarić[37], D. Sobczynska[12], A. Spolon[11], A. Stamerra[3], J. Strišković[30], D. Strom[15], M. Strzys[6], Y. Suda[27], T. Surić[37], M. Takahashi[6], R. Takeishi[6], F. Tavecchio[3], P. Temnikov[34], T. Terzić[23], M. Teshima[15,6], L. Tosti[38], S. Truzzi[13], A. Tutone[3], S. Ubach[26], J. van Scherpenberg[15], G. Vanzo[1], M. Vazquez Acosta[1], S. Ventura[13], V. Verguilov[34], C. F. Vigorito[21], V. Vitale[39], I. Vovk[6], M. Will[15], C. Wunderlich[13], T. Yamamoto[40], and D. Zarić[29]

[1] Instituto de Astrofísica de Canarias and Dpto. de Astrofísica, Universidad de La Laguna, E-38200, La Laguna, Tenerife, Spain [2] Università di Udine and INFN Trieste, I-33100 Udine, Italy [3] National Institute for Astrophysics (INAF), I-00136 Rome, Italy [4] ETH Zürich, CH-8093 Zürich, Switzerland [5] Institut de Física d'Altes Energies (IFAE), The Barcelona Institute of Science and Technology (BIST), E-08193 Bellaterra (Barcelona), Spain [6] Japanese MAGIC Group: Institute for Cosmic Ray Research (ICRR), The University of Tokyo, Kashiwa, 277-8582 Chiba, Japan [7] Technische Universität Dortmund, D-44221 Dortmund, Germany [8] Croatian MAGIC Group: University of Zagreb, Faculty of Electrical Engineering and Computing (FER), 10000 Zagreb, Croatia [9] IPARCOS Institute and EMFTEL Department, Universidad Complutense de Madrid, E-28040 Madrid, Spain [10] Centro Brasileiro de Pesquisas Físicas (CBPF), 22290-180 URCA, Rio de Janeiro (RJ), Brazil [11] Università di Padova and INFN, I-35131 Padova, Italy [12] University of Lodz, Faculty of Physics and Applied Informatics, Department of Astrophysics, 90-236 Lodz, Poland [13] Università di Siena and INFN Pisa, I-53100 Siena, Italy [14] Deutsches Elektronen-Synchrotron (DESY), D-15738 Zeuthen, Germany [15] Max-Planck-Institut für Physik, D-80805 München, Germany [16] Instituto de Astrofísica de Andalucía-CSIC, Glorieta de la Astronomía s/n, 18008, Granada, Spain [17] Università di Pisa and INFN Pisa, I-56126 Pisa, Italy [18] Universitat de Barcelona, ICCUB, IEEC-UB, E-08028 Barcelona, Spain [19] Armenian MAGIC Group: A. Alikhanyan National Science Laboratory, 0036 Yerevan, Armenia [20] Centro de Investigaciones Energéticas, Medioambientales y Tecnológicas, E-28040 Madrid, Spain [21] INFN MAGIC Group: INFN Sezione di Torino and Università degli Studi di Torino, I-10125 Torino, Italy [22] INFN MAGIC Group: INFN Sezione di Bari and Dipartimento Interateneo di Fisica dell'Università e del Politecnico di Bari, I-70125 Bari, Italy [23] Croatian MAGIC Group: University of Rijeka, Department of Physics, 51000 Rijeka, Croatia [24] Universität Würzburg, D-97074 Würzburg, Germany [25] Finnish MAGIC Group: Finnish Centre for Astronomy with ESO, University of Turku, FI-20014 Turku, Finland [26] Departament de Física, and CERES-IEEC, Universitat Autònoma de Barcelona, E-08193 Bellaterra, Spain [27] Japanese MAGIC Group: Physics Program, Graduate School of Advanced Science and Engineering, Hiroshima University, 739-8526 Hiroshima, Japan [28] Armenian MAGIC Group: ICRANet-Armenia at NAS RA, 0019 Yerevan, Armenia [29] Croatian MAGIC Group: University of Split, Faculty of Electrical Engineering, Mechanical Engineering and Naval Architecture (FESB), 21000 Split, Croatia [30] Croatian MAGIC Group: Josip Juraj Strossmayer University of Osijek, Department of Physics, 31000 Osijek, Croatia [31] Japanese MAGIC Group: Department of Physics, Kyoto University, 606-8502 Kyoto, Japan [32] Japanese MAGIC Group: Department of Physics, Tokai University, Hiratsuka, 259-1292 Kanagawa, Japan [33] Saha Institute of Nuclear Physics, HBNI, 1/AF Bidhannagar, Salt Lake, Sector-1, Kolkata 700064, India [34] Inst. for Nucl. Research and Nucl. Energy, Bulgarian Academy of Sciences, BG-1784 Sofia, Bulgaria [35] Japanese MAGIC Group: Department of Physics, Yamagata University, Yamagata 990-8560, Japan [36] Finnish MAGIC Group: Astronomy Research Unit, University of Oulu, FI-90014 Oulu, Finland [37] Croatian MAGIC Group: Ruđer Bošković Institute, 10000 Zagreb, Croatia [38] INFN MAGIC Group: INFN Sezione di Perugia, I-06123 Perugia, Italy [39] INFN MAGIC Group: INFN Roma Tor Vergata, I-00133 Roma, Italy [40] Japanese MAGIC Group: Department of Physics, Konan University, Kobe, Hyogo 658-8501, Japan [41] also at International Center for Relativistic Astrophysics (ICRA), Rome, Italy [42] now at Department for Physics and Technology, University of Bergen, NO-5020, Norway [43] now at University of Innsbruck [44] also at Port d'Informació Científica (PIC), E-08193 Bellaterra (Barcelona), Spain [45] now at Ruhr-Universität Bochum, Fakultät für Physik und Astronomie, Astronomisches Institut (AIRUB), 44801 Bochum, Germany [46] now at Department of Astronomy, University of California Berkeley, Berkeley CA 94720 [47] also at Dipartimento di Fisica, Università di Trieste, I-34127 Trieste, Italy [49] now at Laboratoire d'Annecy de Physique des Particules (LAPP), CNRS-IN2P3, 74941 Annecy Cedex, France [50] also at INAF Trieste and Dept. of Physics and Astronomy, University of

Bologna, Bologna, Italy